



Research article

Impact of pseudoplastic and dilatants behavior of Reiner-Philippoff nanofluid on peristaltic motion with heat and mass transfer analysis in a tapered channel

Muhammad Tahir¹, Yasir Khan^{2,*} and Adeel Ahmad¹

¹ Department of Mathematics, COMSATS University Islamabad, Islamabad 45000, Pakistan

² Department of Mathematics, University of Hafr Al Batin, Hafr Al Batin 31991, Saudi Arabia

***Correspondence:** E-mail: yasirmath@yahoo.com.

Abstract: The main goal of this article is to investigate the effects of pseudoplastic, and dilatants behavior of non-Newtonian based nanofluid on peristaltic motion in an asymmetric tapered channel. Buongiorno's nanofluid model is considered for the study to investigate the heat and mass transfer analysis. The Reiner-Philippoff fluid model is considered to depict the non-Newtonian characteristics of the fluid. The Reiner Philippoff fluid model is the most challenging model among other non-Newtonian fluid models in such a way that shear stress and velocity gradient are non-linearly proportional to each other in this model. This model also represents the implicit relation between stress and deformation rate. The governing equations are based on the dispersion model for nanofluid which incorporates the effects of thermophoretic and Brownian diffusions. The governing equations are simplified in the account of the small Reynolds number and long wavelength assumptions. The solution of the equations is retrieved numerically by the help of built in ND-Solve function of MATHEMATICA software. The sound effects of Reiner-Philippoff based nanofluid on the behavior of velocity and temperature profiles of the fluid, streamlines, pressure gradient fields, and concentration of the nanoparticles are discussed thoroughly. The interesting behavior of Reiner-Philippoff fluid for two limiting shear stress cases when shear stress parameter is very small and very large, for which Reiner-Philippoff fluid behaves like a Newtonian fluid, is also verified. It is observed that fluid flow changes its properties from dilatants fluid to Newtonian and from Newtonian to pseudoplastic fluid by varying the Reiner-Philippoff fluid parameter. According to the findings, the temperature graphs rise against higher thermophoretic diffusion and Brownian motion parameters and falls with higher Prandtl number. Further, the impacts of all the significant parameters are investigated briefly by mathematically as well as graphically.

Keywords: nanofluid; non-Newtonian; Reiner-Philippoff model; peristaltic flow; heat transfer; mass transfer

Mathematics Subject Classification: 35Q79, 76A05, 80A05

Nomenclature

a_1	Amplitude of the upper wall, m ;
Re	Reynolds number;
b_1	Amplitude of the lower wall, m ;
Pr	Prandtl number;
a	Unit-less amplitude of the upper wall;
Ec	Eckert number;
b	Unit-less amplitude of the lower wall;
Br	Brinkman number;
$d_1 + d_2$	Channel width, m ;
S_{ij}	Cauchy stress tensor;
d	Unit-less half channel width;
RPh	Reiner-Philippoff;
(\hat{X}, \hat{Y})	Cartesian coordinates, m ;
\hat{t}	Time, s ;
u	Velocity vector;
t	Unit-less time;
(\hat{U}, \hat{V})	Velocity components, m/s ;
T	Temperature of fluid, K ;
(x, y)	Unit-less Cartesian coordinates;
N_b	Unit-less Brownian parameter;
(u, v)	Unit-less velocity components.

Greek symbols

k_1	Dimensionless non-uniformity parameter;
δ	Wave number, S/m ;
\hat{H}_1	Geometry of the upper wall, m ;
ζ	Phase difference;
\hat{H}_2	Geometry of the lower wall, m ;
λ	Wavelength, m ;
c	Peristaltic wave speed, m/s ;
ψ	Stream function;
h_1	Unit-less geometry of the upper wall;
Φ	Viscous dissipation;
h_2	Unit-less geometry of the lower wall;
λ_1	RPh fluid parameter;
\bar{C}	Specific heat, $J/kg \cdot K$;
ρ	Density, kg/m^3 ;
C	Concentration, mol/m^3 ;
θ	Unit-less temperature;
T_0	Reference temperature at upper wall, K ;
μ	Dynamic viscosity, Ns/m^2 ;
T_1	Reference temperature at lower wall, K ;
ν	Kinematics viscosity;

C_0	Reference concentration at upper wall;
$\hat{\tau}$	Shear stress, N/m^2 ;
C_1	Reference concentration at lower wall;
τ	Dimensionless shear stress;
\hat{P}	Fluid's pressure, N/m^2 ;
$\hat{\tau}_0$	Reference shear stress, N/m^2 ;
p	Dimensionless fluid's pressure;
ϕ	Dimensionless concentration;
\hat{Q}	Instantaneous volumetric flow rate;
α	non-uniformity angle, <i>radian</i> ;
\bar{Q}	Time average flow rate;
γ	Shear stress parameter;
η	Dimensionless mean flow rate;
μ_0	zero shear viscosity, Ns/m^2 ;
D_B	Brownian diffusion coefficient.

Subscripts

D_T	Thermophoretic diffusion coefficient;
f	Base fluid;
K	Thermal conductivity, W/mK ;
p	Nanoparticles;
N_t	Unit-less thermophoretic parameter.

1. Introduction

Demand of getting insight of the peristaltic flow is increasing day by day due to its applications in many fields of science and engineering especially in the fields of biology and medical engineering. Spectrum of research on the topic of peristaltic flow got widen by involving non-Newtonian fluids since most of the fluid involved in different biological systems and other field of engineering are non-Newtonian in nature. Peristalsis is a phenomenon in which the sinusoidal waves arise due to the continuous relaxation and diminution of smooth muscular tissues. Some of the natural and engineering systems involving the application of peristalsis motion are locomotion of earthworm, artificial heart pump, transportation of urine starting from the kidneys to the urinary bladder, vasomotion of tiny blood arteries, motion of the food along the digestive tube and blood transport vessels. The Rotho-peristaltic pump is also one of the applications of peristalsis in chemical industry.

Before Thurston [1], blood was treated as a Newtonian fluid. However, viscoelasticity is a basic rheological property of blood which makes the human blood non-Newtonian. Recently interest in problems of non-Newtonian fluid has grown and many mathematical models for describing the rheological behavior of blood have been extensively developed. Many mathematical structures for elaborating the rheological characteristics of blood have been briefly investigated in references [2–5]. Latham [6] and Shapiro et al. [7] primary reported the fluid dynamical simulation of peristalsis for 2D Newtonian fluid. Tripathi [8] addressed the peristaltic transport of high viscosity across a finite length of channel under the influence of porosity and heat transmission. Hayat et al. [9] explored the significance of hall current on peristaltic flow of Maxwell's fluid passing via porous medium. The latest research on the peristaltic subject can also be seen through references [10–14]. The Reiner-Philippoff fluid model is one of the most challenging non-Newtonian fluid models due to implicit

relationship of shear stress and strain. Due to this mathematical difficulty, limited literature is available on Reiner-Philippoff fluid model. In 1994, Na [15] was the first to examine the boundary layer flow of Reiner-Philippoff fluid due to free stream velocity. The boundary layer flow of Reiner-Philippoff fluid over a stretching sheet was studied by Yam et al. [16] Ahmad [17] investigated the boundary layer flow of Reiner-Philippoff based nanofluid past a non-linear stretching sheet. Impact of Brownian and thermophoresis diffusions on thin film flow of Reiner-Philippoff fluid was studied by Asad Ullah [18]. Sajid et al. [19] investigates the impact of triple diffusive convective flowing on Reiner-Philippoff (RPh) fluid past a stretching surface with Avramenko-Blinov-Shevchuk boundary restrictions. Also Reiner-Philippoff (RPh) fluid model is discussed by considering blood as a base fluid by Sajid et al. [20]. Tahir and Ahmad [21] initiated the study of peristaltic transportation of Reiner-Philippoff fluid.

Heat transfer plays a significant role in equipment efficiency and material selection. The importance of peristaltic fluid motion with heat transfer is noticeable in biomedical sciences, metabolic heat generation, blood transport, perfusion hypothermia, thermoregulation and in bio-heat exchange processes. The working capability of every biological and mechanical process decays time to time due to the production of heat by such processes. To improve the efficiency of such mechanism it is compulsory to eliminate the heat regularly from the system. Nanofluids are innovative compounds that can control the heat transfer. Nanofluids are made by nanoprecipitation method in ordinary fluids. The ordinary fluids like water, polymer solutions, engine oil and some lubricants have less thermal conductivity values as compared to solids. Including a specific quantity of solid particles to these fluids, can easily enhance the heat conductance of these fluids. These particles are usually of sizes ranging 1–100 nanometer and known as nanoparticles. The consequential mixture of fluid and nanoparticles is called nanofluid. This idea of constructing nanofluids was primarily introduced by Choi [22,23] in 1995. Xuan [24] talked about the improvements of heat transfers for nanofluids. Buongiorno [25] proposed a model that incorporates thermophoresis and Brownian motion phenomena to evaluate the transport of nanofluids. Nanofluids are also helpful and applicable in the understanding of a variety of phenomenon such as the minimization/enhancement of the thermal magnitude of the system, microchannel clogging, miniaturization of the system and minimal clogging. Recently Rasool et al. [26] investigates and provides a numerical analysis of electro-magneto-hydrodynamic (EMHD) nanofluid flows past a Riga pattern embedded horizontally in a Darcy-Forchheimer porous medium. The more literature regarding heat transfer through nanofluids can be seen through references [27–33]. Many academics are interested in the combined impacts of heat and mass transfer because of its vast spectrum of uses in industry, science, and engineering. These procedures play a critical role in enhancing the product quality. They're used in a variety of pharmaceutical and chemical operations, as well as magnetic drug targeting and electronic devices cooling. Thermal insulation, thermal energy storage, fossil fuel extraction, the paper industry, food processing, oxygenation, porous solid drying, hemodialysis, subterranean energy transmission and geothermal energy recovery are some additional physical examples. Hina [34] in 2012 explored how the compliant walls affected peristaltic flow, heat transfer, mass transport and chemical reactions. Peristaltic movement study of Eyring-Prandtl fluid in a tube together with heat and mass transfer analysis was investigated by Iftikhar et al. [35]. Researcher's contributions to peristaltic flows are fast expanding due to the relevance of heat and mass transport in several fields of engineering and science (see citations [36–39]).

As discussed earlier that negligible research was available on non-Newtonian Reiner-Philippoff fluid model. And particularly no literature was available on peristaltic motion of Reiner-Philippoff fluid. In previous work [40] heat transfer analysis of Renner-Philippoff nanofluid was discussed by

using conventional nanofluid model. Considering the importance of non-Newtonian fluid in peristaltic flow and role of nanoparticles as an efficient agent of heat transfer control, the aim of this article is to explore heat and mass transfer analysis of non-Newtonian Reiner-Philippoff fluid in peristaltic motion in the presence of nanoparticles by using Buongiorno's nanofluid model. The impact of thermophoretic diffusion parameter, Brownian diffusion parameter and Reiner-Philippoff fluid parameter on different quantities of interest is discussed in detail. I hope this study will be step forward in the field of peristaltic flow, heat and mass transfer of non-Newtonian fluids and also provides new avenues of research for scholars to the way of RPh fluid academics.

2. Mathematical analysis

Consider Reiner-Philippoff (RPh) fluid flowing through a non-uniform (tapered) two-dimensional asymmetric channel to be incompressible. The fluid movement is caused by the sinusoidal waves having wavelength λ and constant speed c along the channel walls. The walls of the non-uniform channel are separated by width $d_1(\hat{X}) + d_2(\hat{X})$. The coordinate system for the given problem is Cartesian system (\hat{X}, \hat{Y}) introduced in such a way that $\hat{Y} - axis$ is chosen alongside the width and the $\hat{X} - axis$ is along the length of the channel. Geometrical deformation of the walls for discussed problem can be put mathematically as [41]:

$$\hat{H}_1(\hat{X}, \hat{t}) = d_1(\hat{X}, \hat{t}) + a_1 \cos\left(\frac{2\pi}{\lambda}(\hat{X} - c\hat{t})\right), \text{ upper wall} \quad (1)$$

$$\hat{H}_2(\hat{X}, \hat{t}) = -d_2(\hat{X}, \hat{t}) - b_1 \cos\left(\frac{2\pi}{\lambda}(\hat{X} - c\hat{t}) + \zeta\right), \text{ lower wall}, \quad (2)$$

where, $d_i(\hat{X}, \hat{t}) = d_i + (\hat{X} - c\hat{t})\tan(\alpha)$, ($i=1,2$), is the half width of channel, α is the non-uniformity angle of the channel, $\hat{H}_1(\hat{X}, \hat{t})$ and $\hat{H}_2(\hat{X}, \hat{t})$ symbolized to show the geometry of the said problem for topper and lower walls respectively corresponding to the coordinate $\hat{Y} > 0$ and $\hat{Y} < 0$. a_1 and b_1 are the amplitudes of the topper and lower waves respectively, \hat{t} is for the time and ζ ($0 \leq \zeta \leq \pi$) represents phase difference between the waves, for $\zeta = 0$ the channel is reduced to symmetric in which waves are totally out of phase and for $\zeta = \pi$ waves are totally in phase (see Figure 1). Superscript $\hat{\cdot}$ is used to indicate the dimensional quantities. Further, d_1, a_1, d_2 and b_1 satisfies the following [42]:

$$a_1^2 + b_1^2 + 2 a_1^2 b_1^2 \cos \zeta \leq (d_1 + d_2)^2. \quad (3)$$

Two-dimensional velocity fields are taken with the velocity components as $\hat{U}(\hat{X}, \hat{Y}, \hat{t})$ and $\hat{V}(\hat{X}, \hat{Y}, \hat{t})$ along the $\hat{X} - axis$ and $\hat{Y} - axis$ respectively.

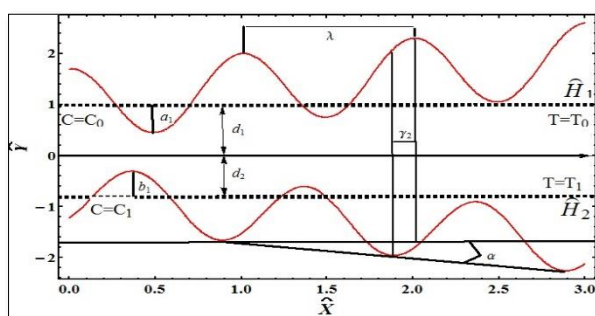


Figure 1. Geometrical interpretation of the problem.

The governing equations for an incompressible RPh fluid flow can be expressed as the following set of equations [43]:

$$\nabla \cdot \mathbf{u} = 0, \quad (4)$$

$$\rho \frac{D\mathbf{u}}{Dt} = \nabla \cdot \mathbf{S}_{ij}, \quad (5)$$

$$(\rho \bar{C})_f \frac{DT}{Dt} = K_f \nabla^2 T + \Phi + (\rho \bar{C})_p \left(D_B (\nabla C \cdot \nabla T) + D_T \frac{\nabla C \cdot \nabla T}{T_m} \right), \quad (6)$$

$$\frac{DC}{Dt} = \frac{D_T}{T_m} \nabla^2 T + D_B \nabla^2 C, \quad (7)$$

where, ρ_f signifies the base fluid density and ρ_p is the density of particles, $\mathbf{u} = u(\hat{U}(\hat{X}, \hat{Y}, \hat{t}), \hat{V}(\hat{X}, \hat{Y}, \hat{t}), 0)$ indicate velocity vectors, \hat{t} is for time, \bar{C}_f is specific heat of base fluid and \bar{C}_p is particles specific heat, K_f indicates the thermal conductivity, T is temperature, C is concentration, D_B and D_T are stands for Brownian and thermophoretic diffusion coefficients respectively. \mathbf{S}_{ij} and Φ are the Cauchy stress tensor and viscous dissipation terms and are given as [44]:

$$\mathbf{S}_{ij} = -\hat{P}I + \hat{\tau}_{ij}, \quad (8)$$

$$\Phi = (\hat{\tau}_{\hat{Y}\hat{Y}} - \hat{\tau}_{\hat{X}\hat{X}}) \frac{\partial \hat{V}}{\partial \hat{Y}} + \hat{\tau}_{\hat{X}\hat{Y}} \left(\frac{\partial \hat{U}}{\partial \hat{Y}} + \frac{\partial \hat{V}}{\partial \hat{X}} \right). \quad (9)$$

Where for the Reiner-Philippoff (RPh) fluid model, the stress strain relation is specified as [18]:

$$\hat{\tau}_{ij} = \left[\mu_\infty + \frac{\mu_0 - \mu_\infty}{1 + \left(\frac{1}{2\hat{\tau}_0^2} \right) (\sum_{l=1}^2 \sum_{m=1}^2 \hat{\tau}_{lm} \hat{\tau}_{ml})} \right] \hat{e}_{ij}, \quad (10)$$

with,

$$\begin{aligned} \sum_{l=1}^2 \sum_{m=1}^2 \hat{\tau}_{lm} \hat{\tau}_{ml} &= \sum_{l=1}^2 [\hat{\tau}_{l1} \hat{\tau}_{1l} + \hat{\tau}_{l2} \hat{\tau}_{2l}] \\ &= \hat{\tau}_{11} \hat{\tau}_{11} + \hat{\tau}_{21} \hat{\tau}_{12} + \hat{\tau}_{12} \hat{\tau}_{21} + \hat{\tau}_{22} \hat{\tau}_{22} \\ &= \hat{\tau}_{11}^2 + 2\hat{\tau}_{12}^2 + \hat{\tau}_{22}^2. \end{aligned}$$

Using $\hat{\tau}_{12} = \hat{\tau}_{21}$.

The RPh fluid model (Eq (10)) contain three positive parameters μ_∞ , μ_0 and $\hat{\tau}_0$. Here μ_∞ represents the higher Newtonian limiting viscosity, μ_0 is the viscosity at zero shear stress rate and $\hat{\tau}_0$ indicates the reference shear stress.

In two dimensional Cartesian coordinates system, the continuity Eq (4), momentum Eq (5), the thermal energy Eq (6) and the concentration Eq (7) in laboratory frame are expressed as:

$$\frac{\partial \hat{U}}{\partial \hat{X}} + \frac{\partial \hat{V}}{\partial \hat{Y}} = 0, \quad (11)$$

$$(\rho_f) \left(\frac{\partial}{\partial \hat{t}} + \hat{U} \frac{\partial}{\partial \hat{X}} + \hat{V} \frac{\partial}{\partial \hat{Y}} \right) \hat{U} = -\frac{\partial \hat{P}}{\partial \hat{X}} + \frac{\partial \hat{\tau}_{\hat{X}\hat{X}}}{\partial \hat{X}} + \frac{\partial \hat{\tau}_{\hat{X}\hat{Y}}}{\partial \hat{Y}}, \quad (12)$$

$$(\rho_f) \left(\frac{\partial}{\partial \hat{t}} + \hat{U} \frac{\partial}{\partial \hat{X}} + \hat{V} \frac{\partial}{\partial \hat{Y}} \right) \hat{V} = -\frac{\partial \hat{P}}{\partial \hat{Y}} + \frac{\partial \hat{\tau}_{\hat{Y}\hat{X}}}{\partial \hat{X}} + \frac{\partial \hat{\tau}_{\hat{Y}\hat{Y}}}{\partial \hat{Y}}, \quad (13)$$

$$\begin{aligned} \rho_f \bar{C}_f \left(\frac{\partial T}{\partial \hat{t}} + \hat{U} \frac{\partial T}{\partial \hat{X}} + \hat{V} \frac{\partial T}{\partial \hat{Y}} \right) &= K_f \left(\frac{\partial^2 T}{\partial \hat{X}^2} + \frac{\partial^2 T}{\partial \hat{Y}^2} \right) + \left[(\hat{\tau}_{\hat{Y}\hat{Y}} - \hat{\tau}_{\hat{X}\hat{X}}) \frac{\partial \hat{V}}{\partial \hat{Y}} + \hat{\tau}_{\hat{X}\hat{Y}} \left(\frac{\partial \hat{U}}{\partial \hat{Y}} + \frac{\partial \hat{V}}{\partial \hat{X}} \right) \right] \\ &\quad + \Gamma \rho_f \bar{C}_f \left[D_B \left(\frac{\partial T}{\partial \hat{Y}} \frac{\partial C}{\partial \hat{Y}} + \frac{\partial C}{\partial \hat{X}} \frac{\partial T}{\partial \hat{X}} \right) + \frac{D_T}{T_m} \left(\frac{\partial T}{\partial \hat{X}} + \frac{\partial T}{\partial \hat{Y}} \right)^2 \right], \end{aligned} \quad (14)$$

$$\left(\frac{\partial}{\partial \hat{t}} + \hat{U} \frac{\partial}{\partial \hat{X}} + \hat{V} \frac{\partial}{\partial \hat{Y}} \right) C = \frac{D_T}{T_m} \left(\frac{\partial^2 T}{\partial \hat{X}^2} + \frac{\partial^2 T}{\partial \hat{Y}^2} \right) + D_B \left(\frac{\partial^2 C}{\partial \hat{X}^2} + \frac{\partial^2 C}{\partial \hat{Y}^2} \right), \quad (15)$$

where, $\Gamma = \frac{\rho_p \bar{C}_p}{\rho_f \bar{C}_f}$ and Eq (10) in component form can be written as:

$$\hat{\tau}_{\hat{X}\hat{X}} = \left[\mu_{\infty} + \frac{\mu_0 - \mu_{\infty}}{1 + \left(\frac{1}{2\hat{\tau}_0^2}\right)(\hat{\tau}_{\hat{X}\hat{X}}^2 + 2\hat{\tau}_{\hat{X}\hat{Y}}^2 + \hat{\tau}_{\hat{Y}\hat{Y}}^2)} \right] \hat{e}_{\hat{X}\hat{X}}, \quad (16)$$

$$\hat{\tau}_{\hat{X}\hat{Y}} = \left[\mu_{\infty} + \frac{\mu_0 - \mu_{\infty}}{1 + \left(\frac{1}{2\hat{\tau}_0^2}\right)(\hat{\tau}_{\hat{X}\hat{X}}^2 + 2\hat{\tau}_{\hat{X}\hat{Y}}^2 + \hat{\tau}_{\hat{Y}\hat{Y}}^2)} \right] \hat{e}_{\hat{X}\hat{Y}}, \quad (17)$$

$$\hat{\tau}_{\hat{Y}\hat{Y}} = \left[\mu_{\infty} + \frac{\mu_0 - \mu_{\infty}}{1 + \left(\frac{1}{2\hat{\tau}_0^2}\right)(\hat{\tau}_{\hat{X}\hat{X}}^2 + 2\hat{\tau}_{\hat{X}\hat{Y}}^2 + \hat{\tau}_{\hat{Y}\hat{Y}}^2)} \right] \hat{e}_{\hat{Y}\hat{Y}}, \quad (18)$$

where,

$$\hat{e}_{\hat{X}\hat{X}} = 2 \cdot \frac{\partial \hat{U}}{\partial \hat{X}}, \hat{e}_{\hat{Y}\hat{Y}} = 2 \cdot \frac{\partial \hat{V}}{\partial \hat{Y}} \text{ and } \hat{e}_{\hat{X}\hat{Y}} = \left(\frac{\partial \hat{V}}{\partial \hat{X}} + \frac{\partial \hat{U}}{\partial \hat{Y}} \right). \quad (19)$$

The subsequent transformations are used to change the investigated problem from stationary reference frame to moving frame [45]:

$$\begin{cases} \hat{x} = \hat{X} - c\hat{t}, \\ \hat{y} = \hat{Y}, \\ \hat{v}(\hat{x}, \hat{y}) = \hat{V}(\hat{X}, \hat{Y}, \hat{t}) \\ \hat{p}(\hat{x}, \hat{y}) = \hat{P}(\hat{X}, \hat{Y}, \hat{t}) \\ \hat{u}(\hat{x}, \hat{y}) = \hat{U}(\hat{X}, \hat{Y}, \hat{t}) - c \end{cases} \quad (20)$$

And the following dimensionless quantities are used to convert the above dimensional system in dimensionless form:

$$\begin{cases} x = \frac{\hat{x}}{\lambda}, y = \frac{\hat{y}}{d_1}, t = \frac{c\hat{t}}{\lambda}, u = \frac{\hat{u}}{c}, v = \frac{\hat{v}}{c\delta}, \\ \delta = \frac{d_1}{\lambda}, \tau_{ij} = \frac{d_1 \hat{\tau}_{ij}}{c\mu_f}, p = \frac{d_1^2 \hat{p}}{c\mu_f \lambda}, h_1 = \frac{\hat{H}_1}{d_1}, h_2 = \frac{\hat{H}_2}{d_1}, \\ a = \frac{a_1}{d_1}, b = \frac{b_1}{d_1}, d = \frac{d_2}{d_1}, \nu = \frac{\mu_f}{\rho_f}, \\ \text{Pr} = \frac{\mu_f c_f}{K_f}, \text{Re} = \frac{cd_1 \rho_f}{\mu_f}, \text{Ec} = \frac{c^2}{c_f \Delta T}, \text{Br} = \text{Pr} \cdot \text{Ec}, \\ \theta = \frac{T - T_m}{T_1 - T_0}, \phi = \frac{C - C_m}{C_1 - C_0}, N_b = \Gamma \frac{D_B(C_1 - C_0)}{\nu}, N_t = \Gamma \frac{D_T(T_1 - T_0)}{\nu T_m}. \end{cases} \quad (21)$$

Here h_1 and h_2 represents the dimension free forms of both walls, ν is kinematics viscosity, d is the channel width ratio, ϕ indicates the concentration of nanoparticles, N_b is the parameter of Brownian motion, N_t is indicate the thermophoresis diffusion parameter, θ correspond to dimension free temperature, Pr, Re, Ec and Br are the Prandtl number, Reynolds number, Eckert number and Brinkman number respectively.

The dimensionless form of the governing equations in the wave frame in accounts of Eq (20) and the quantities (21) is as:

$$\frac{\partial u}{\partial x} + \frac{\partial v}{\partial y} = 0, \quad (22)$$

$$\delta \text{Re} \left\{ \left[\frac{\partial}{\partial t} + (u+1) \frac{\partial}{\partial x} + v \frac{\partial}{\partial y} \right] (u+1) \right\} = -\frac{\partial p}{\partial x} + \delta \left(\frac{\partial \tau_{xx}}{\partial x} \right) + \frac{\partial \tau_{xy}}{\partial y}, \quad (23)$$

$$\delta^3 \text{Re} \left\{ \left[\frac{\partial}{\partial t} + (u+1) \frac{\partial}{\partial x} + v \frac{\partial}{\partial y} \right] v \right\} = -\frac{\partial p}{\partial y} + \delta^2 \left(\frac{\partial \tau_{yx}}{\partial x} \right) + \delta \frac{\partial \tau_{yy}}{\partial y}, \quad (24)$$

$$\begin{aligned} & \delta \text{RePr} \left\{ \left[\frac{\partial \theta}{\partial t} + (u+1) \frac{\partial \theta}{\partial x} + v \frac{\partial \theta}{\partial y} \right] \right\} \\ &= \left(\delta^2 \frac{\partial^2 \theta}{\partial x^2} + \frac{\partial^2 \theta}{\partial y^2} \right) + \delta Br (\tau_{yy} - \tau_{xx}) \frac{\partial v}{\partial y} + Br \tau_{xy} \left(\frac{\partial u}{\partial y} + \delta^2 \frac{\partial v}{\partial x} \right) \\ &+ \text{Pr} N_b \left(\frac{\partial \theta}{\partial y} \frac{\partial \phi}{\partial y} + \delta^2 \frac{\partial \phi}{\partial x} \frac{\partial \theta}{\partial x} \right) + \text{Pr} N_b \left(\delta^2 \frac{\partial \theta}{\partial x} + \frac{\partial \theta}{\partial y} \right)^2, \end{aligned} \quad (25)$$

$$\delta \text{Re}(\Delta C.\Gamma) \left[\frac{\partial \phi}{\partial t} + (u+1) \frac{\partial \phi}{\partial x} + v \frac{\partial \phi}{\partial y} \right] = N_t \left(\delta^2 \frac{\partial^2 \theta}{\partial x^2} + \frac{\partial^2 \theta}{\partial y^2} \right) + N_b \left(\delta^2 \frac{\partial^2 \phi}{\partial x^2} + \frac{\partial^2 \phi}{\partial y^2} \right), \quad (26)$$

and corresponding dimensionless form of Eqs (16)–(18) are as under:

$$\tau_{xx} = \delta \left[1 + \frac{\lambda_1 - 1}{1 + \frac{1}{2\tau_0^2} (\tau_{xx}^2 + 2\tau_{xy}^2 + \tau_{yy}^2)} \right] \frac{\partial u}{\partial x}, \quad (27)$$

$$\tau_{yy} = \delta \left[1 + \frac{\lambda_1 - 1}{1 + \frac{1}{2\tau_0^2} (\tau_{xx}^2 + 2\tau_{xy}^2 + \tau_{yy}^2)} \right] \frac{\partial v}{\partial y}, \quad (28)$$

$$\tau_{xy} = \left[1 + \frac{\lambda_1 - 1}{1 + \frac{1}{2\tau_0^2} (\tau_{xx}^2 + 2\tau_{xy}^2 + \tau_{yy}^2)} \right] \frac{\partial u}{\partial y}. \quad (29)$$

In above equations $\lambda_1 = \frac{\mu_0}{\mu_\infty}$. Now by using the estimations of lengthy wavelength ($\delta \ll 1$), small Reynolds number and by using the description of following stream functions:

$$u = \frac{\partial \psi}{\partial y} \quad \text{and} \quad v = -\frac{\partial \psi}{\partial x}. \quad (30)$$

Equation (22) satisfies identically and Eqs (23)–(29) simplifies to the following form:

$$\frac{\partial p}{\partial x} = \frac{\partial}{\partial y} \tau_{xy}, \quad (31)$$

$$\frac{\partial p}{\partial y} = 0, \quad (32)$$

$$\frac{\partial^2 \theta}{\partial y^2} + Br \tau_{xy} \left(\frac{\partial^2 \psi}{\partial y^2} \right) + \text{Pr} N_b \left(\frac{\partial \theta}{\partial y} \frac{\partial \phi}{\partial y} \right) + \text{Pr} N_t \left(\frac{\partial \theta}{\partial y} \right)^2 = 0, \quad (33)$$

$$\frac{N_b}{N_t} \left(\frac{\partial^2 \phi}{\partial y^2} \right) + \frac{\partial^2 \theta}{\partial y^2} = 0, \quad (34)$$

$$\tau_{xx} = 0 \quad \text{and} \quad \tau_{yy} = 0, \quad (35)$$

and

$$\tau_{xy} = \left(1 + \frac{\lambda_1 - 1}{1 + \left(\frac{\tau_{xy}^2}{\tau_0^2} \right)} \right) \frac{\partial^2 \psi}{\partial y^2}. \quad (36)$$

From Eqs (31) and (32) we have:

$$\frac{\partial^2}{\partial y^2} \tau_{xy} = 0. \quad (37)$$

Which depicts that τ_{xy} is a linear function of y and can be written as $\tau_{xy} = A_1 y + B_1$, where A_1 and B_1 are arbitrary parameters. And Eq (36) can be written as:

$$\frac{\partial^2 \psi}{\partial y^2} = \tau_{xy} \left[\frac{\gamma + \tau_{xy}^2}{\tau_{xy}^2 + \gamma \lambda_1} \right]. \quad (38)$$

This is explicit relationship between deformation rate and shear stress for RPh nanofluid. Where, $\lambda_1 = \frac{\mu_0}{\mu_\infty}$ and $\gamma = \tau_0^2$ are RPh fluid parameter and shear stress parameter respectively. For $\lambda_1 = 1$ this relation converges to Newtonian fluid.

The dimension freeform of the walls $h_1(x)$ and $h_2(x)$ are is given as:

$$\begin{cases} h_1(x) = 1 + k_1x + a \cos[2\pi x], \\ h_2(x) = -d - k_1x - b \cos[2\pi x + \zeta], \end{cases} \quad (39)$$

where, $k_1 = \frac{\lambda \tan \alpha}{d_1}$ is the non-uniformity parameter of the channel.

2.1. Pumping characteristics

The instantaneous volumetric flow rate in the laboratory frame of reference is given by:

$$\hat{Q}(\hat{X}, \hat{t}) = \int_{\hat{h}_2}^{\hat{h}_1} \hat{U}(\hat{X}, \hat{Y}, \hat{t}) d\hat{Y}, \quad (40)$$

where, \hat{H}_1 and \hat{H}_2 are the functions of \hat{X} and \hat{t} . Now using Eq (19), Eq (40) becomes:

$$\hat{Q}(\hat{X}, \hat{t}) = \int_{\hat{h}_2}^{\hat{h}_1} \hat{u}(\hat{x}, \hat{y}) d\hat{y} + c(\hat{h}_1 - \hat{h}_2) = \hat{q} + c(\hat{h}_1 - \hat{h}_2), \quad (41)$$

where, $\hat{h}_1(\hat{x})$ and $\hat{h}_2(\hat{x})$ represents the upper, lower channel walls for wave frame and $\hat{q}(\hat{x}, \hat{y})$ is the instantaneous volumetric flow rate in the moving frame and is given by:

$$\hat{q}(\hat{x}, \hat{y}) = \int_{\hat{h}_2}^{\hat{h}_1} \hat{u}(\hat{x}, \hat{y}) d\hat{y}. \quad (42)$$

The time average flow rate (over one period T) is given by:

$$\bar{Q} = \frac{1}{T} \int_0^T \hat{Q} d\hat{t}. \quad (43)$$

Using Eq (41) in Eq (43) we have:

$$\begin{aligned} \bar{Q} &= \frac{1}{T} \int_0^T \hat{q} d\hat{t} + c(\hat{h}_1 - \hat{h}_2) \\ &= \hat{q} + cd_1 + cd_2 + 2c\hat{x}\lambda \tan \alpha \\ &\quad + ca_1 \cos\left(\frac{2\pi}{\lambda} \hat{x}\right) + cb_1 \cos\left(\frac{2\pi}{\lambda} \hat{x} + \zeta\right). \end{aligned} \quad (44)$$

We note that $h_1(x)$ and $h_2(x)$ given in Eq (39) are the corresponding dimension free forms of the non-uniform peristaltic channel. So the corresponding dimension free form of Eq (44) is given as:

$$\eta = F + 1 + d + 2k_1x + a \cos(2\pi x) + b \cos(2\pi x + \zeta), \quad (45)$$

where, $\eta = \frac{\bar{Q}}{cd_1}$ and $F = \frac{\hat{q}}{cd_1}$ are the dimension free mean flow rates in the fixed and moving frame respectively and the expression of F is given as:

$$F = \int_{h_2}^{h_1} u(x, y) dy = \int_{h_2}^{h_1} \frac{\partial \psi}{\partial y} dy = \psi(h_1) - \psi(h_2). \quad (46)$$

The associated dimensionless boundary conditions are:

$$\begin{cases} \psi = \frac{F}{2}, \psi' = -1, \theta = -0.5, \phi = -0.5 \text{ at upper wall } h_1(x), \\ \psi = \frac{-F}{2}, \psi' = -1, \theta = 0.5, \phi = 0.5 \text{ at lower wall } h_2(x). \end{cases} \quad (47)$$

3. Result and discussions

Equation (32) depicts that the expression of the pressure function is free from 'y' variable and Eq (37) demonstrates that τ_{xy} is a linear function of 'y'. Thus the solution of Eqs (33), (34) and (38) corresponding to the boundary conditions given in Eq (47) is retrieved numerically by the help of built in NDSolve

function of MATHEMATICA software. Outcomes of the study are discussed thoroughly by plotting the graphs in rest of this section. We will talk about the effects of RPh nanofluid properties on physical quantities of interest like the axial velocity u , streamline functions ψ , concentration of nanoparticles ϕ , temperature profiles θ , heat transfer rate $-\theta'(h)$ and mass transportation rate $-\phi'(h)$ at the upper boundary and pressure gradient $\frac{dp}{dx}$.

3.1. Axial velocity

Graphical visualization of velocity profiles against dissimilar values of RPh fluid parameter λ_1 , shear stress parameter γ , for both pseudoplastic and dilatants fluids and arbitrary parameter A_1 is shown in Figures 2–5. Reiner-Philippoff (RPh) fluid behaves like dilatants fluid for $\lambda_1 < 1$, as pseudoplastic for $\lambda_1 > 1$ and as Newtonian fluid for $\lambda_1 = 1$. The influence of RPh fluid parameter λ_1 on the fluid's velocity profiles is drawing in Figure 2 the blue line in the figure against the value $\lambda_1 = 1$ is showing the velocity of Newtonian fluid. Further it is shown that the maximum velocity for pseudoplastic (shear thinning) fluid, corresponding to the value $\lambda_1 > 1$, is larger than the velocity of dilatants fluid corresponding to the value of $\lambda_1 < 1$. As RPh fluid proceeds as shear thinning (pseudoplastic) fluid for the value $\lambda_1 > 1$, therefore its viscosity decreases as compared to shear thickening (dilatants) fluid and that's why the fluid's deformation rate increases and consequently velocity profile improves. RPh fluid model (see Eq (36)) behaves like Newtonian fluid for extreme shear rates. The same case is analyzed in Figures 3 and 4. From these two figures we can see that for $\gamma \rightarrow 0$ and for $\gamma \rightarrow \infty$. in both cases the fluid's velocity is same for both pseudoplastic ($\lambda_1 = 2.0$) and dilatants ($\lambda_1 = 0.25$) fluid. The other survey from these two graphs is that velocity is increasing function of shear stress parameter γ for pseudoplastic fluid and decreasing function for dilatants fluid. As in shear thinning case, fluid decreases its viscosity against applied shear stress and in case of shear thickening fluid, fluid gains viscosity that's why in case of pseudoplastic fluid velocity increases and in case of dilatants fluid velocity decreases against shear stress parameter. Figure 5 depicts that by escalating the value of arbitrary parameter A_1 the fluid's velocity increase. Initially this increment is notable but after that there is no significant effect of arbitrary parameter A_1 on velocity graph.

3.2. Temperature

This section covers physical assessment of parameters like RPh fluid parameter λ_1 shear stress parameter γ , Brownian motion parameter N_b , thermophoresis diffusion parameter N_t , Brinkman number Br and Prandtl number Pr on temperature profiles. As a result, Figures 6–12 are required to look for such an analysis briefly. Figure 6 demonstrates that by ascending the value of RPh fluid parameter λ_1 the fluid's temperature increases. As at $\lambda_1 = 1$ the fluid behaves like the Newtonian fluid. And so the study shows that in same circumstances the temperature for dilatants fluid is less than the Newtonian's fluid temperature and Newtonian's fluid temperature is smaller than the pseudoplastic fluid's temperature. In Figures 7 and 8 the influences of shear stress parameter γ are deliberated on temperature profiles for pseudoplastic and dilatants fluids respectively. These graphs reveal that the temperature is an increasing function of shear stress parameter γ for pseudoplastic fluids and it behaves totally opposite for dilatants fluids for same values of shear stress parameter γ as decreasing function. The relevance of Brinkman's number on fluid hotness can be seen through Figure 9. This figure proves that fluid becomes hotter by enlarging the value of Brinkman number. Because the Brinkman number occurs as a result of viscous dissipation therefore, extra heat is created with greater Brinkman number, and therefore the temperature rises and hence temperature profile get enlarged. Also see reference [45]. Figure 10 represents that for greater Brownian motion parameter the

temperature of the liquid increases. The consequence of Brownian scale tends to increase the relative mobility of nanoparticles compounds from the walls to the substance in response to which an increment in the temperature profile occurs. Figure 11 confirms a similar pattern of temperature distributions in relation to the thermophoresis parameter N_t . Physically greater N_t implies the occurrence of temperature differential phenomenon in which high-temperature nanoparticles transported to cooler region of the channel. As a result temperature is intensified. Figure 12 signifies that by increasing the amount of Prandtl number Pr the temperature of the nanofluid also increases. Because Prandtl number Pr has direct connection with specific heat of the liquid so increased specific heat raise the temperature of fluid.

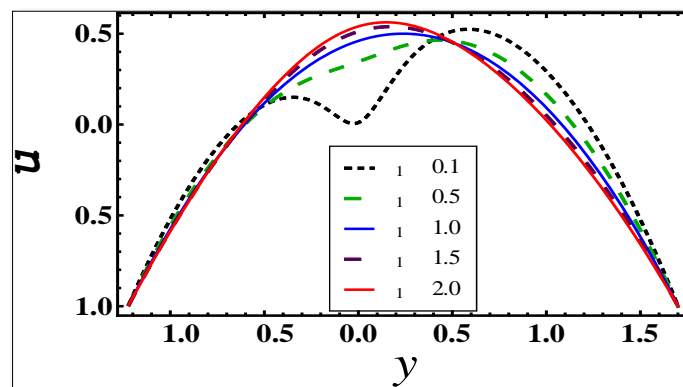


Figure 2. Velocity profiles against dissimilar values of λ_1 ($\gamma = 1, k_1 = 0.1, a = 0.7, d = 0.8, A_1 = 2, b = 0.6, B_1 = 1, \eta = 1.5, x = 0, \zeta = \frac{\pi}{4}$).

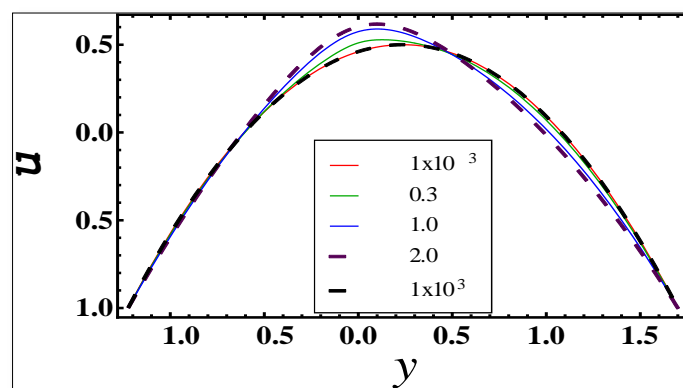


Figure 3. Velocity profiles of pseudoplastic fluid against dissimilar values of γ ($\lambda_1 = 2, k_1 = 0.1, a = 0.7, d = 0.8, A_1 = 2, b = 0.6, B_1 = 1, \eta = 1.5, x = 0, \zeta = \frac{\pi}{4}$).

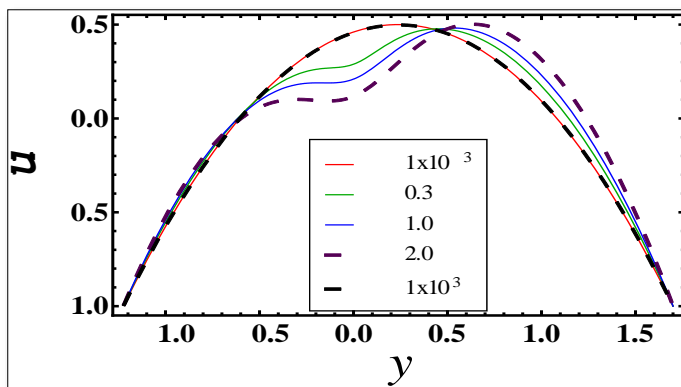


Figure 4. Velocity profiles of dilatant fluid against dissimilar values of γ ($\lambda_1 = 0.25, a = 0.7, d = 0.8, A_1 = 2, b = 0.6, B_1 = 1, \eta = 1.5, x = 0, \zeta = \frac{\pi}{4}$).

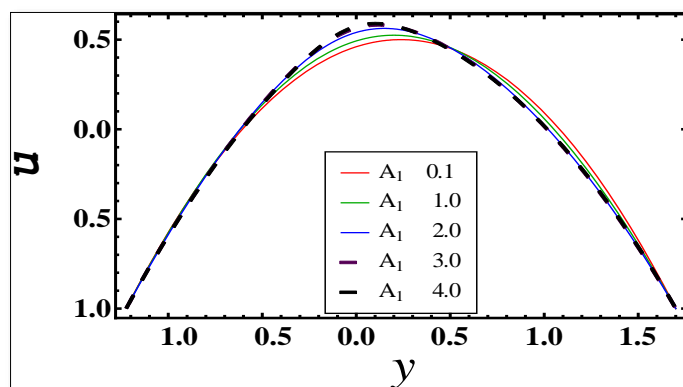


Figure 5. Velocity profiles against dissimilar values of A_1 ($\gamma = 1, k_1 = 0.1, a = 0.7, d = 0.8, \lambda_1 = 2, b = 0.6, B_1 = 1, \eta = 1.5, x = 0, \zeta = \frac{\pi}{4}$).

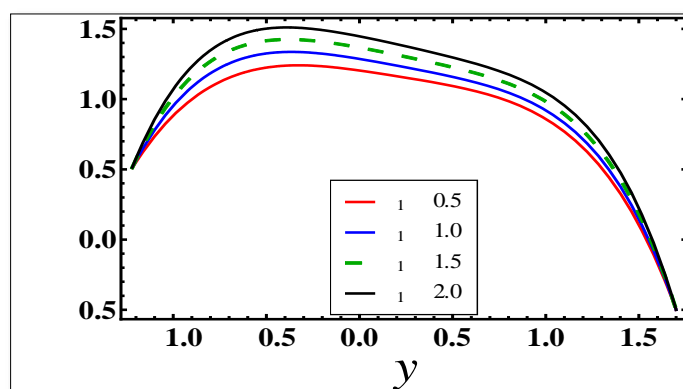


Figure 6. Temperature profiles against dissimilar values of λ_1 ($\gamma = 1, k_1 = 0.1, a = 0.7, d = 0.8, b = 0.6, A_1 = 2, B_1 = 1, \eta = 1.5, x = 0, \zeta = \frac{\pi}{4, Br=1.5, Pr=1.0, N_t=0.5, N_b=0.5}$).

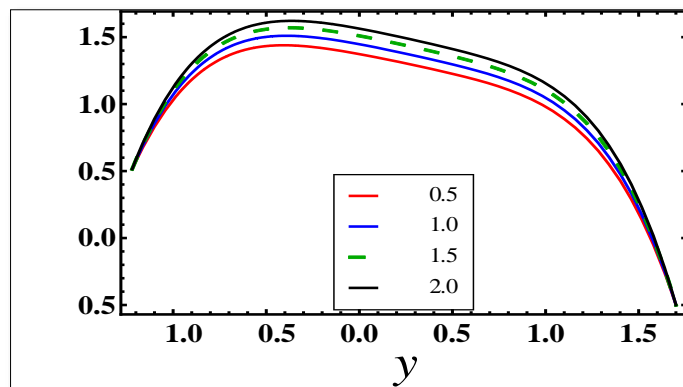


Figure 7. Temperature profiles of pseudoplastic fluid against dissimilar values of γ ($\lambda_1 = 2, k_1 = 0.1, a = 0.7, b = 0.6, d = 0.8, A_1 = 2, B_1 = 1, \eta = 1.5, x = 0, \zeta = \frac{\pi}{4}, Br = 1.5, Pr = 1.0, N_t = 0.5, N_b = 0.5$).

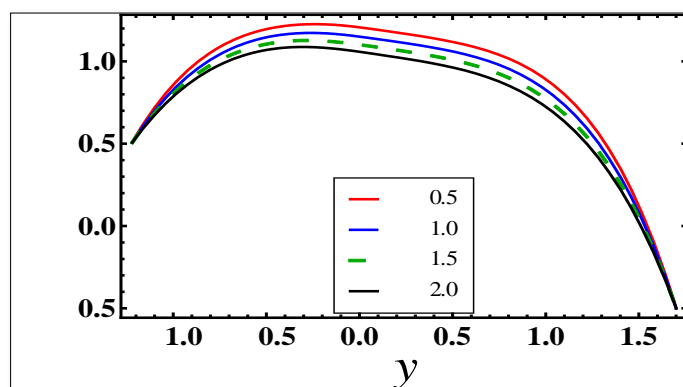


Figure 8. Temperature profiles of dilatants fluid against dissimilar values of γ ($\lambda_1 = 0.25, N_t = 0.5, k_1 = 0.1, a = 0.7, d = 0.8, A_1 = 2, b = 0.6, B_1 = 1, \eta = 1.5, x = 0, \zeta = \frac{\pi}{4}, Br = 1.5, Pr = 1.0, N_b = 0.5$).

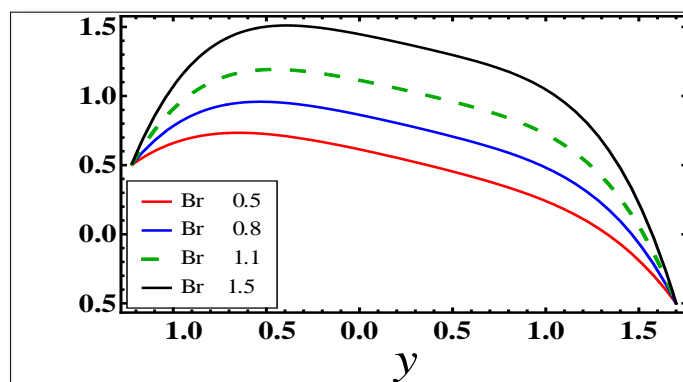


Figure 9. Temperature profiles against dissimilar values of Br number. ($\gamma = 1, k_1 = 0.1, a = 0.7, d = 0.8, A_1 = 2, b = 0.6, B_1 = 1, \eta = 1.5, x = 0, \zeta = \frac{\pi}{4}, \lambda_1 = 2, Pr = 1.0, N_t = 0.5, N_b = 0.5$).

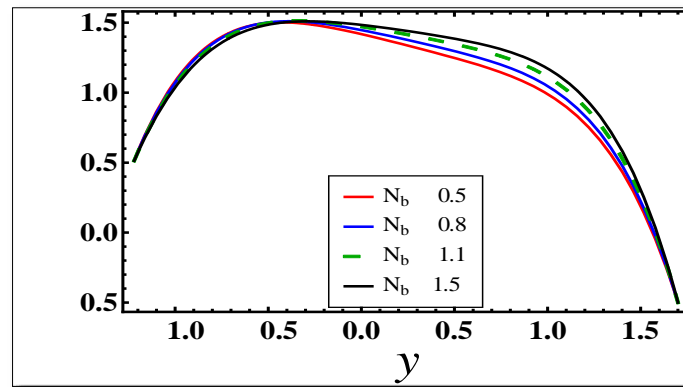


Figure 10. Temperature profiles against dissimilar values of N_b ($\gamma = 1, a = 0.7, a = 0.7, k_1 = 0.1, b = 0.6, A_1 = 2, B_1 = 1, \eta = 1.5, x = 0, \zeta = \frac{\pi}{4, Br=1.5, Pr=1.0, N_t=0.5, \lambda_1=2}$).

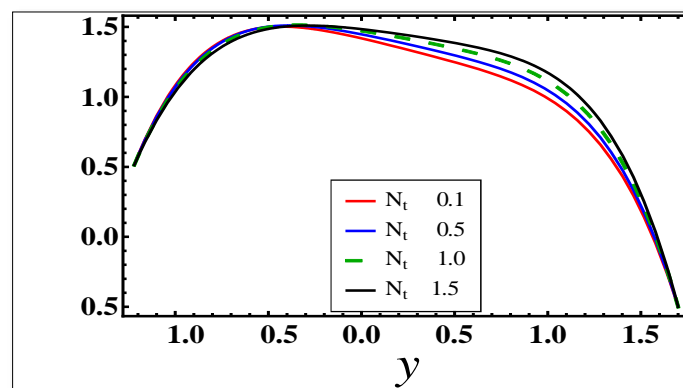


Figure 11. Temperature profiles against dissimilar values of N_t ($\gamma = 1, a = 0.7, d = 0.8, k_1 = 0.1, b = 0.6, A_1 = 2, B_1 = 1, \eta = 1.5, x = 0, \zeta = \frac{\pi}{4, Br=1.5, Pr=1.0, \lambda_1=2, N_b=0.5}$).

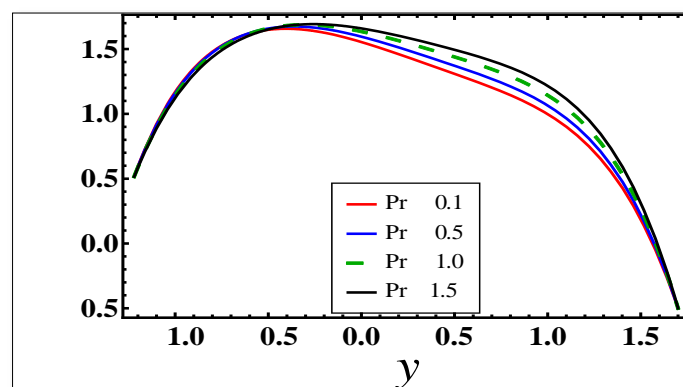


Figure 12. Temperature profiles against dissimilar values of Pr number ($\gamma = 1, a = 0.7, k_1 = 0.1, b = 0.6, d = 0.8, A_1 = 2, B_1 = 1, \eta = 1.5, x = 0, \zeta = \frac{\pi}{4, Br=1.5, \lambda_1=2, N_t=0.5, N_b=0.5}$).

3.3. Concentration

The influence of sundry factors on the concentration of nanoparticles graphs are scrutinized through Figures 13 to 19. These graphs pointed out that the concentration of nanoparticles at the center of the channel is highly effected by the changing the values of implanted parameters. Figure 13 is plotted to show the effect of RPh fluid parameter λ_1 on the concentration of nanoparticles. A decreasing tendency in nanoparticles mass transport rate is observed for enhancing values of λ_1 . From this we can conclude that concentration of nanoparticles for dilatants fluids is larger as compared to pseudoplastic fluids. Shear stress parameter γ have opposite concern on concentration for pseudoplastic and dilatants fluid which can be seen through Figures 14 and 15. For pseudoplastic fluids the concentration of nanoparticles is decreasing graph of shear stress parameter while for dilatants fluids it depicts increasing behavior. Figure 16 illustrates that with an increment in Brinkman number Br results with a decrease in nanoparticles mass transfer. Figures 17 and 18 reveal the antagonistic effects of Brownian motion parameter N_b and thermophoretic diffusions parameter N_t on concentration graphs. Declining impact is marked by ϕ for increasing thermophoretic diffusion parameter because with the strength of thermophoretic forces the action of diffusion is turned on which depressed the concentration profile of nanofluid. Contrary to this a rising effect in concentration is achieved by enhancing Brownian motion as nanoparticles attained higher densities for stronger Brownian motion which in turn develops concentration. Figure 19 depicts the Prandtl number Pr effects on concentration profile. From figure we can see that by growing values of Prandtl number Pr yields a depressed behavior of concentration profiles near the upper wall but this observation is not hold near lower wall where the significance of Pr is directly proportional to concentration profile.

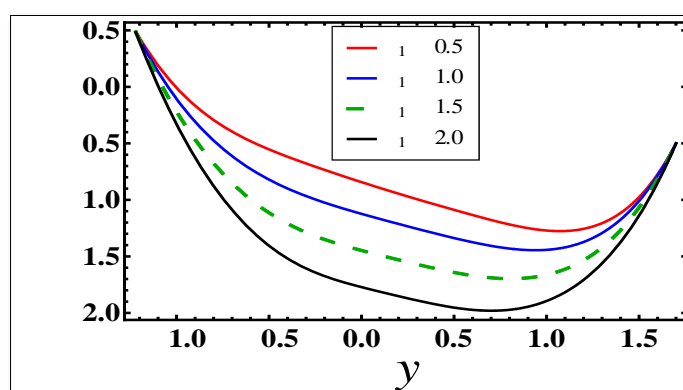


Figure 13. Concentration profiles against dissimilar values of λ_1 ($\gamma = 1, k_1 = 0.1, a = 0.7, b = 0.6, d = 0.8, A_1 = 2, B_1 = 1, \eta = 1.5, x = 0, \zeta = \frac{\pi}{4, Br=1.5, Pr=1.0, N_b=0.5, N_t=0.5}$).

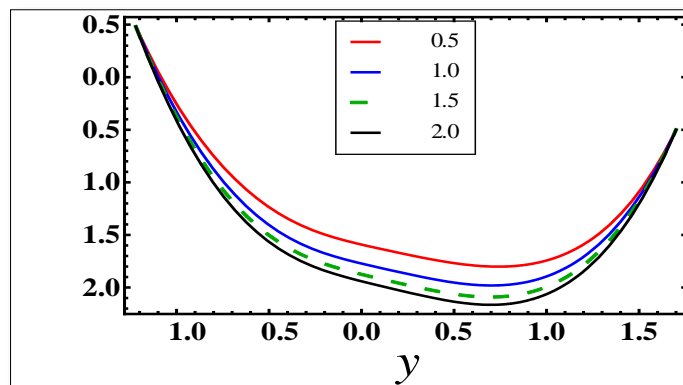


Figure 14. Concentration profiles of pseudoplastic fluid against dissimilar values of γ ($\lambda_1 = 2, k_1 = 0.1, a = 0.7, d = 0.8, A_1 = 2, b = 0.6, B_1 = 1, \eta = 1.5, x = 0, \zeta = \frac{\pi}{4}, Br = 1.5, Pr = 1.0, N_t = 0.5, N_b = 0.5$).

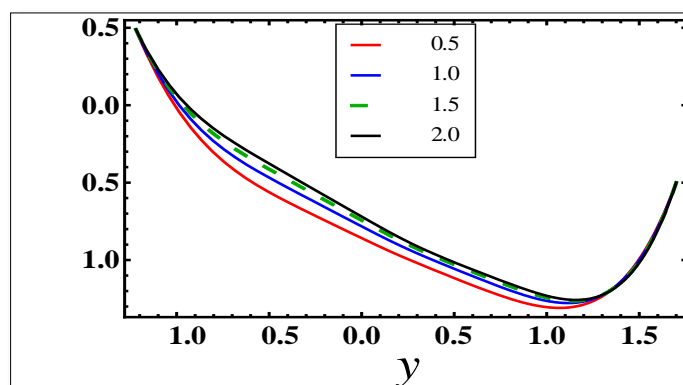


Figure 15. Concentration profiles of dilatants fluid against dissimilar values of γ ($\lambda_1 = 0.25, k_1 = 0.1, a = 0.7, d = 0.8, A_1 = 2, b = 0.6, B_1 = 1, \eta = 1.5, \zeta = \frac{\pi}{4}, Br = 1.5, Pr = 1.0, N_t = 0.5, N_b = 0.5$).

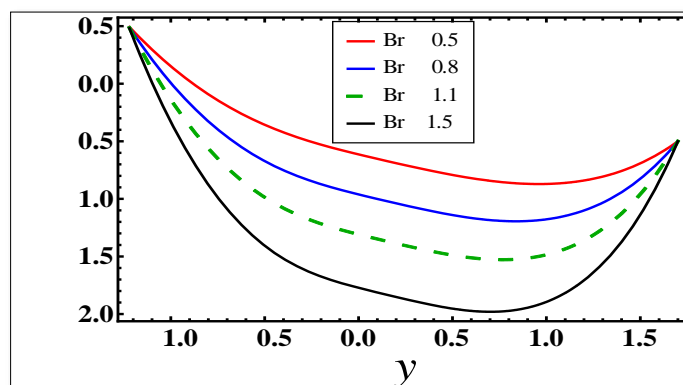


Figure 16. Concentration profiles against dissimilar values of Br number ($\gamma = 1, k_1 = 0.1, a = 0.7, b = 0.6, d = 0.8, A_1 = 2, B_1 = 1, \eta = 1.5, x = 0, \zeta = \frac{\pi}{4}, \lambda_1 = 2, Pr = 1.0, N_b = 0.5, N_t = 0.5$).

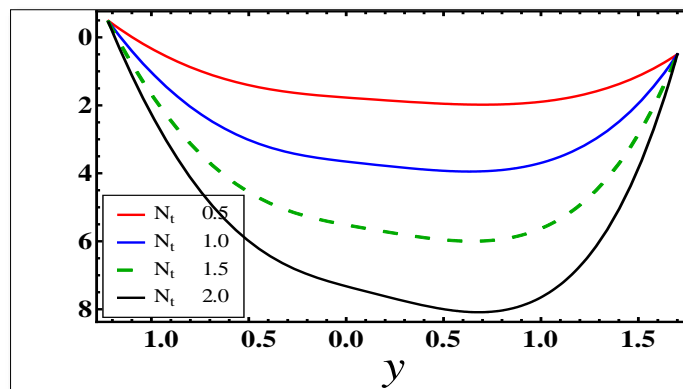


Figure 17. Concentration profiles against dissimilar values of N_t ($\gamma = 1, k_1 = 0.1, a = 0.7, b = 0.6, d = 0.8, A_1 = 2, B_1 = 1, \eta = 1.5, x = 0, \zeta = \frac{\pi}{4, Br=1.5, Pr=1.0, \lambda_1=2, N_b=0.5}$).

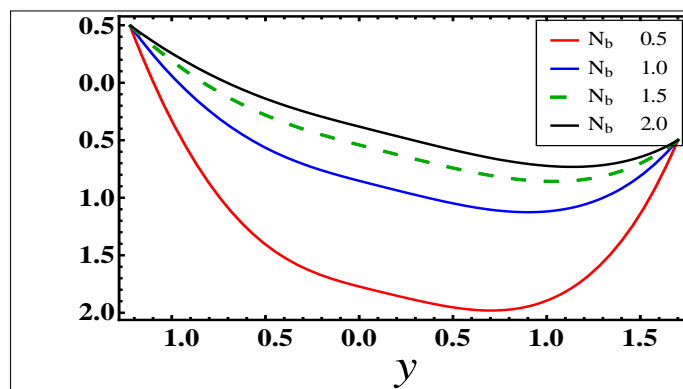


Figure 18. Concentration profiles against dissimilar values of N_b ($\gamma = 1, k_1 = 0.1, a = 0.7, d = 0.8, A_1 = 2, b = 0.6, B_1 = 1, \eta = 1.5, x = 0, \zeta = \frac{\pi}{4, Br=1.5, Pr=1.0, N_t=0.5, \lambda_1=2}$).

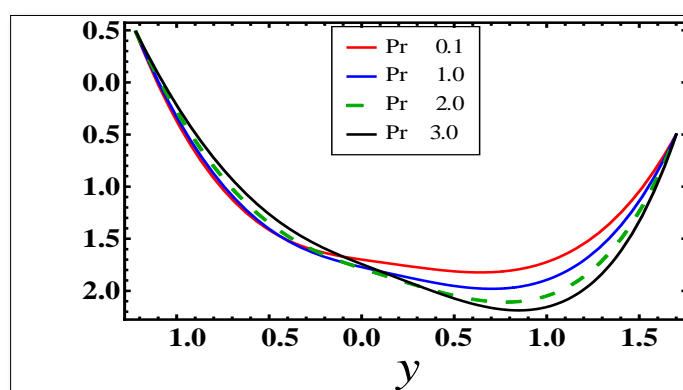


Figure 19. Concentration profiles against dissimilar values of Pr ($\gamma = 1, k_1 = 0.1, a = 0.7, d = 0.8, A_1 = 2, b = 0.6, B_1 = 1, \eta = 1.5, x = 0, \zeta = \frac{\pi}{4, Br=1.5, \lambda_1=2, N_t=0.5, N_b=0.5}$).

3.4. Pressure gradient

In Figures 20–23 we will discuss about the effects of λ_1, γ and k_1 on the pressure gradient profiles within channel. The common observation from these graphs is that the pressure gradient gains its maximum value at the narrowest section of the channel. Figure 20 demonstrates that by intensifying the value of λ_1 the pressure gradient of RPh nanofluid increases. The rising behavior of pressure gradient field is larger in the contracted as compared to the broader section of the channel. In this figure the blue thick line is the representation of Newtonian fluid's pressure gradient. The lines upper the blue lines against the values $\lambda_1 > 1$ correspond to the pseudoplastic fluid and the lines below the blue line against the values $\lambda_1 < 1$ characterized the dilatants fluid. In Figure 21 the significance of γ on the pressure gradient is evaluated for shear thinning fluid. It is investigated from this sketch that pressure gradient of RPh fluid raises by increasing the value of γ . In Figure 22 the same significance of γ on pressure gradient is studied for the dilatants fluid. The influence of γ on pressure gradient for dilatants fluid is quite dissimilar as compared to the pseudoplastic fluid. In the case of dilatants, by increasing the value of γ the amount of pressure gradient reduces. Figure 23 examined that for $k_1 = 0$, the height of every crest of the pressure gradient is same at narrow section of the channel. However, as we increase the value of parameter k_1 , that is, when we increase the width of channel, the height of each succeeding crest of the pressure gradient decreases than the preceding crest. This is because of by adding the value of k_1 the width of the channel increases and so the pressure gradient decreases in the wider part. This whole phenomenon can be seen in Figure 23.

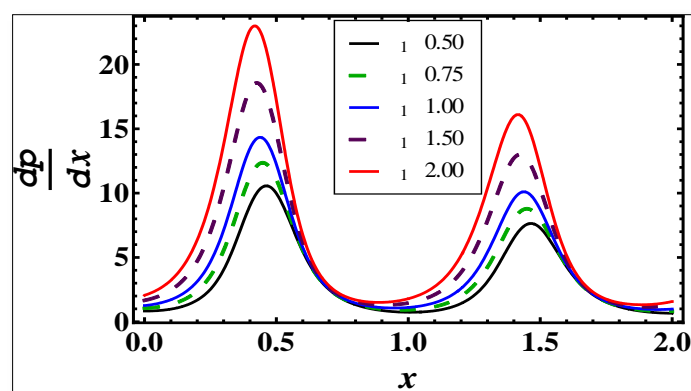


Figure 20. Pressure gradient profiles against dissimilar values of λ_1 ($\gamma = 1, k_1 = 0.1, a = 0.7, d = 0.8, A_1 = 2, b = 0.6, B_1 = 1, \eta = 1.5, \zeta = \frac{\pi}{4}$).

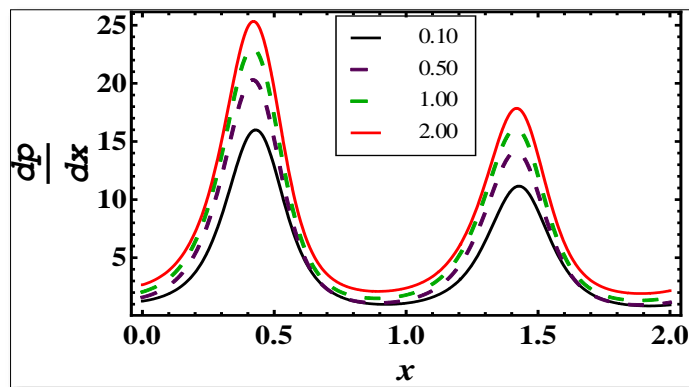


Figure 21. Pressure gradient profiles of pseudoplastic fluid against dissimilar values of γ ($\lambda_1 = 2, k_1 = 0.1, a = 0.7, d = 0.8, A_1 = 2, b = 0.6, B_1 = 1, \eta = 1.5, \zeta = \frac{\pi}{4}$).

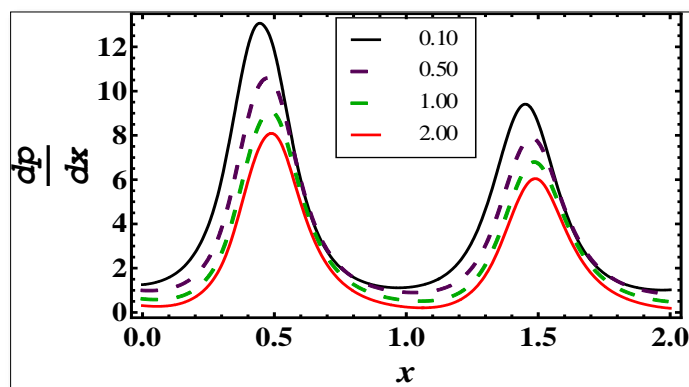


Figure 22. Pressure gradient profiles of dilatant fluid against dissimilar values of γ ($\lambda_1 = 0.25, k_1 = 0.1, a = 0.7, d = 0.8, A_1 = 2, b = 0.6, B_1 = 1, \eta = 1.5, \zeta = \frac{\pi}{4}$).

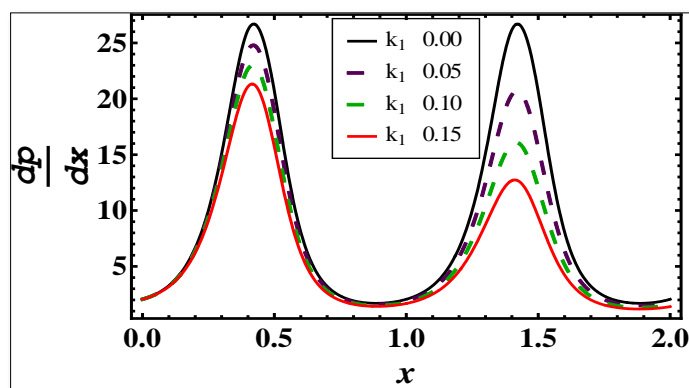


Figure 23. Pressure gradient profiles against dissimilar values of k_1 ($\gamma = 1, \lambda_1 = 2, a = 0.7, b = 0.6, d = 0.8, A_1 = 2, B_1 = 1, \eta = 1.5, \zeta = \frac{\pi}{4}$).

3.5. Streamlines

This part consists of the physical study of parameters like RPh fluid parameter λ_1 , phase difference of the waves ζ , shear stress parameter γ and non-uniformity parameter k_1 on stream line contours. From Figure 24, it is experimented that by improving the value of λ_1 the size of the bolus increases. Bolus is the result of fluid's trapped volume by streamlines with the motion of the fluid, this generates an intriguing phenomenon known as trapping, the construction of an inner flowing bolus of nanofluid which moved together with the waves with wave speed at a fixed mean flow rate. Figure 25 indicates that phase difference of the channel has opposite effect on fluid trapped volume than the λ_1 as by increasing the angle of phase difference, the volume of the bolus decreases. Figures 26 and 27 are drawn to understand the impact shear stress parameter γ on streamline functions for shear thinning fluids and shear thickening fluids respectively. From Figure 26 we can see that bolus for pseudoplastic fluids have increasing behavior with greater shear stress parameter. As this fluid is shear thinning fluid so by increasing shear stress parameter the fluid's viscosity decreases and fluid moves more freely, and more fluid's volume get trapped. Contrary to this fluid the size of bolus decreases in case of dilatants fluids for same values of shear stress parameter as we can observe from Figure 27. Figure 28 signifies that the amount of trapping volume of fluid get increases by increasing the non-uniformity of the channel and consequently the dimension of the bolus get increased.

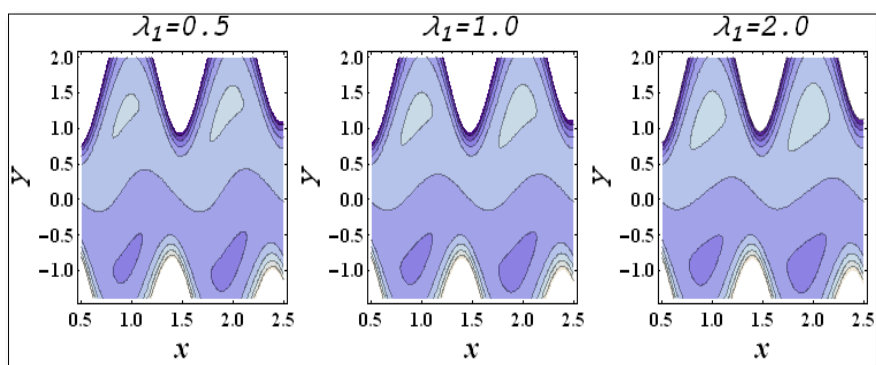


Figure 24. Streamline graphs against dissimilar values of λ_1 ($\gamma = 1, k_1 = 0.1, a = 0.7, d = 0.8, A_1 = 2, b = 0.6, B_1 = 1, \eta = 2.0, \zeta = \frac{\pi}{4}$).

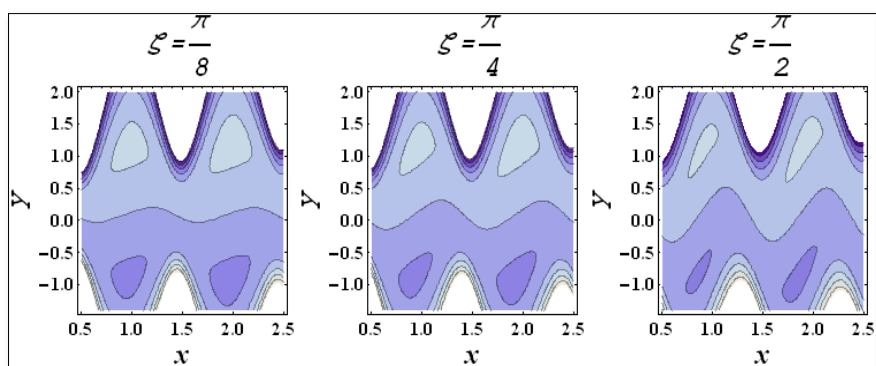


Figure 25. Streamline graphs against dissimilar values of ζ ($\gamma = 1, k_1 = 0.1, a = 0.7, d = 0.8, A_1 = 2, b = 0.6, B_1 = 1, \eta = 2.0, \lambda_1 = 2$).

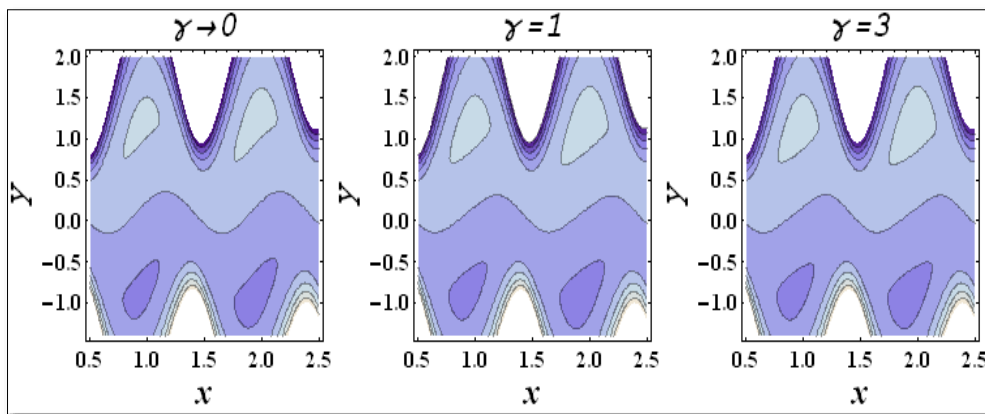


Figure 26. Streamline graphs of pseudoplastic fluid against dissimilar values of γ ($\lambda_1 = 2, k_1 = 0.1, a = 0.7, d = 0.8, A_1 = 2, b = 0.6, B_1 = 1, \eta = 2.0, \zeta = \frac{\pi}{4}$).

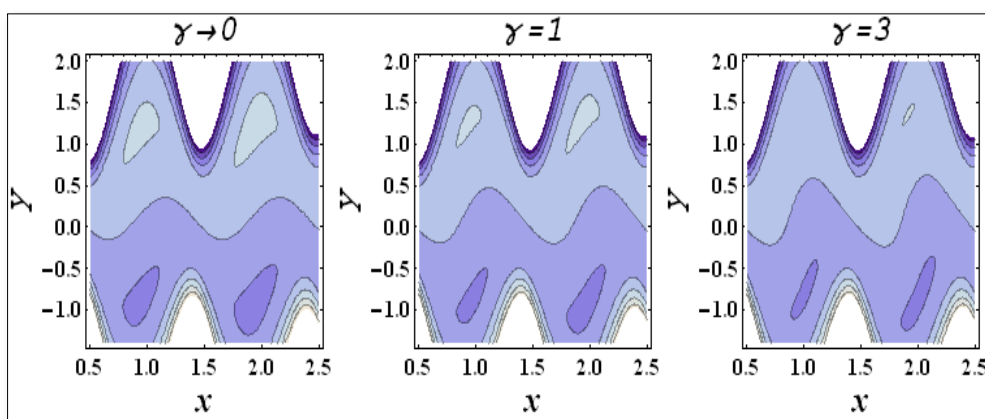


Figure 27. Streamline graphs of dilatant fluid against dissimilar values of γ ($\lambda_1 = 0.25, k_1 = 0.1, a = 0.7, d = 0.8, A_1 = 2, b = 0.6, B_1 = 1, \eta = 2.0, \zeta = \frac{\pi}{4}$).

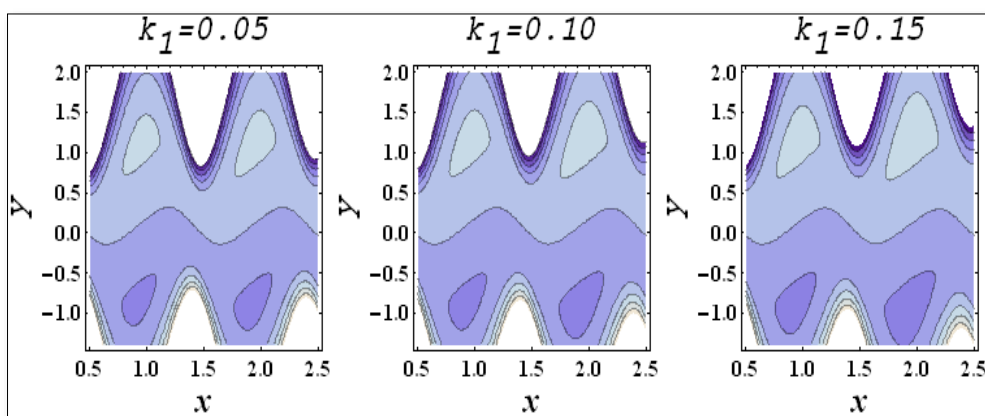


Figure 28. Streamline graphs against dissimilar values of k_1 ($\gamma = 1, \lambda_1 = 2, a = 0.7, d = 0.8, A_1 = 2, b = 0.6, B_1 = 1, \eta = 2.0, \zeta = \frac{\pi}{4}$).

3.6. Heat and mass transfer rates

Table 1 presents the numerical assessment of heat and mass transfer rates at the upper border of the channel for various physical parameters. First four lines of the table exhibits that heat transfer ($-\theta'(h_1)$) and mass transfer ($-\phi'(h_1)$) rates are increasing function of RPh fluid parameter λ_1 , which concludes that RPh fluid parameter improves heat and mass transfer process between the solid boundaries and the base fluid. Secondly, the table 1 predicts that in case of shear thinning fluids, heat ($-\theta'(h_1)$) and mass transfer ($-\phi'(h_1)$) rates raise for greater shear stress parameter and on the other hand for shear thickening fluid these transfer rates decline. Next four lines represent that heat transfer ($-\theta'(h_1)$) and mass transfer ($-\phi'(h_1)$) rates are increases by enlarging N_t . Moreover the ratio of mass transfer ($-\phi'(h_1)$) is much significant as compared to heat transfer ($-\theta'(h_1)$) rate. The table's following four lines anticipated that the Brownian motion parameter has opposing impacts on heat ($-\theta'(h_1)$) and mass transfer ($-\phi'(h_1)$) rates. As with increased Brownian motion parameter, the mass transfer rate ($-\phi'(h_1)$) drops drastically while the heat transfer rate ($-\theta'(h_1)$) increases steadily. The very next four lines of the table demonstrate that the Brinkman's number has a direct influence on heat ($-\theta'(h_1)$) and mass transfer ($-\phi'(h_1)$) rates. As by enlarging the Brinkman number, both the heat ($-\theta'(h_1)$) and mass transport ($-\phi'(h_1)$) rates improved. The last four lines of the table reveals that raising the Prandtl number improved the heat ($-\theta'(h_1)$) and mass transfer ($-\phi'(h_1)$) rates.

Table 1. Numerical measurements of heat and mass transfer rates at the channel's upper border for various parameters.

λ_1	γ	N_t	N_b	Br	Pr	$-\theta'(h_1)$	$-\phi'(h_1)$
0.5	1.0	0.8	0.8	1.5	1.0	3.94339	3.25946
1.0						4.24148	3.55755
1.5						4.52987	3.84593
2.0						4.81133	4.12740
1.5	0.5					4.39119	3.70726
	1.0					4.52987	3.84593
	1.5					4.64350	3.95957
	2.0					4.73910	4.05516
0.5	0.5					4.09858	3.41464
	1.0					4.94339	3.25946
	1.5					4.81863	3.13470
	2.0					3.71590	3.03197
1.5	1.0	0.4				4.30704	1.64057
		0.8				4.52987	3.84593
		1.2				4.75514	6.27779
		1.6				4.98124	8.93658
		0.8	0.4			4.30703	7.58817
			0.8			4.52987	3.84593
			1.2			4.75514	2.60015
			1.6			4.98124	1.97764
			0.8	0.5		1.66990	1.28304
				1.0		3.28843	2.56540

Continued on next page

λ_1	γ	N_t	N_b	Br	Pr	$-\theta'(h_1)$	$-\phi'(h_1)$
				1.5		4.52987	3.84593
				2.0		5.81130	5.12737
				1.5	0.5	4.08841	3.40448
					1.0	4.52987	3.84593
					1.5	4.98124	4.29731
					2.0	5.43078	7.74984

4. Conclusions

Peristaltic flow of non-Newtonian based nanofluid in a tapered asymmetric channel is examined in this research. The governing equations incorporates dispersion model for the nanofluid and RPh fluid model for non-Newtonian fluid. Simplified form of governing equation based on long wavelength and small Reynolds number approximations are solved numerically. The consequential effects of different physical quantities on the velocity of the nanofluid, pressure gradient, temperature and concentration profiles are portrayed graphically. The most important outcomes of the study are given below:

- Velocity is increasing function of shear stress parameter for pseudoplastic fluid and decreasing function of shear stress parameter for dilatants fluid.
- It is noted that by increasing the value of RPh fluid parameter λ_1 the temperature of the nanofluid increases.
- It is worth noting that both thermophoretic and Brownian diffusions causes temperature graphs to climb.
- A decreasing tendency in nanoparticles mass transfer is observed for enhancing values of RPh fluid parameter. From this we can conclude that concentration of nanoparticles for dilatants fluid is greater as compared to pseudoplastic fluid.
- Thermophoretic diffusion and Brownian motion factors have opposing influence on concentration of nanoparticles profiles. Concentration graph decreases by increasing thermophoretic diffusion parameter and increases by enhancing Brownian motion parameter.
- Further it is noticed that the addition of Brinkman number results in an enhancement in the nanofluid temperature.
- The pressure gradient of the nanofluid is higher in the occluded section of the channel as compared to the broader section of the channel.
- By increasing the non-uniformity of the channel, the pressure gradient of the nanofluid decreases as the width of the channel increases.
- The addition in the value of RPh fluid parameter λ_1 the trapped volume of the nanofluid increases.
- It is also important to observe that the RPh fluid parameter enables heat and mass transfer rates to increase.
- Brownian motion parameter has opposing impacts on heat and mass transfer rates. As with increased Brownian motion parameter, the mass transfer rate drops drastically while the heat transfer rate increases steadily.
- It is analyzed from the study represented that heat transfer and mass transfer rates are increased by enlarging the thermophoretic diffusion parameter.

I hope this study will be step forward in the field of peristaltic flow, heat and mass transfer of non-Newtonian fluids and also provides new avenues of research for scholars to the way of RPh fluid academics.

Acknowledgments

This research work was funded by institutional fund projects under no. (IFP-A-2022-2-5-24). Therefore, authors gratefully acknowledge technical and financial support from the ministry of education and University of Hafr Al Batin, Saudi Arabia.

Conflict of interest

The authors declare no conflict of interest.

References

1. G. B. Thurston, N. M. Henderson, M. Jeng, Effects of erythrocytapheresis transfusion on the viscoelasticity of sickle cell blood, *Clin. Hemorheol. Microcirc.*, **30** (2004), 83–97.
2. H. A. Baieth, S. Hamza, Comparative examination of constitutive equations for apparent viscosity of human blood, *Egypt. J. Biophys. Biomed. Eng.*, **7** (2006), 85–96.
3. G. Pedrzzetti, L. Zavatto, F. Domenichini, A. Tortoriello, Pulstile flow inside moderately elastic arteries, its modeling and effects of elasticity, *Comput. Methods Biomec. Biomed. Eng.*, **5** (2002), 219–231. <http://doi.org/10.1080/10255840212874>
4. G. Pontrelli, Nonlinear problems in arterial flows, *Nonlinear Anal.*, **47** (2001), 4905–4915. [https://doi.org/10.1016/S0362-546X\(01\)00603-4](https://doi.org/10.1016/S0362-546X(01)00603-4)
5. F. J. Walburn, D. J. Scnech, A constitutive equation for whole human blood, *Biorheology*, **13** (1976), 201–210. <https://doi.org/10.3233/bir-1976-13307>
6. T. W. Latham, Fluid motion in a peristaltic pump, In: *Massachusetts Institute of Technology*, Massachusetts Institute of Technology, 1966.
7. A. H. Shapiro, M. Y. Jaffrin, S. L. Weinberg, Peristaltic pumping with long wavelengths at low Reynolds number, *J. Fluid Mech.*, **37** (1969), 799–825. <https://doi.org/10.1017/S0022112069000899>
8. D. Tripathi, Study of transient peristaltic heat flow through a finite porous channel, *Math. Comput. Model.*, **57** (2013), 1270–1283. <https://doi.org/10.1016/j.mcm.2012.10.030>
9. T. Hayat, N. Ali, S. Asghar, Hall effects on peristaltic flow of a Maxwell fluid in a porous medium, *Phys. Lett. A*, **363** (2007) 397–403. <https://doi.org/10.1016/j.physleta.2006.10.104>
10. S. A. Hussein, S. E. Ahmed, A. A. Arafa, Electrokinetic peristaltic bioconvective Jeffrey nanofluid flow with activation energy for binary chemical reaction, radiation and variable fluid properties, *ZAMM-Z. Angew. Math. Me.*, 2022, e202200284. <https://doi.org/10.1002/zamm.202200284>
11. M. G. Reddy, K. V. Reddy, O. D. Makinde, Hydromagnetic peristaltic motion of a reacting and radiating couple stress fluid in an inclined asymmetric channel filled with a porous medium, *Alex. Eng. J.*, **55** (2016), 1841–1853. <https://doi.org/10.1016/j.aej.2016.04.010>
12. A. A. Arafa, S. E. Ahmed, M. M. Allan, Peristaltic flow of non-homogeneous nanofluids through variable porosity and heat generating porous media with viscous dissipation: Entropy analyses, *Case Stud. Therm. Eng.*, **32** (2022), 101882. <https://doi.org/10.1016/j.csite.2022.101882>

13. T. Anwar, M. Tahir, P. Kumam, S. Ahmed, P. Thounthong, Magnetohydrodynamic mixed convective peristaltic slip transport of carbon nanotubes dispersed in water through an inclined channel with Joule heating, *Heat Transf.*, **50** (2020), 2064–2089. <https://doi.org/10.1002/htj.21969>
14. B. B. Divya, G. Manjunatha, C. Rajashekhar, H. Vaidya, K. V. Prasad, The hemodynamics of variable liquid properties on the MHD peristaltic mechanism of Jeffery fluid with heat and mass transfer, *Alex. Eng. J.*, **59** (2020), 693–706. <https://doi.org/10.1016/j.aej.2020.01.038>
15. T. Y. Na, Boundary layer flow of Reiner-Philippoff fluids, *Internat. J. Non-Linear Mech.*, **29** (1994), 871–877. [https://doi.org/10.1016/0020-7462\(94\)90059-0](https://doi.org/10.1016/0020-7462(94)90059-0)
16. K. S. Yam, S. D. Herris, D. B. Ingham, I. Pop, Boundary-layer flow of Reiner-Philippoff fluids past a stretching wedge, *Internat. J. Non-Linear Mech.*, **44** (2009), 1056–1062. <https://doi.org/10.1016/j.ijnonlinmec.2009.08.006>
17. A. Ahmad, Flow of Reiner-Philippoff based nano-fluid past a stretching sheet, *J. Mol. Liq.*, **219** (2016), 643–646. <https://doi.org/10.1016/j.molliq.2016.03.068>
18. A. Ullah, E. O. Alzahrani, Z. Shah, M. Ayaz, S. Islam, Nanofluid's thin film flow of Reiner-Philippoff fluid over an unstable stretching surface with Brownian motion and thermophoresis effects, *Coatings*, **9** (2019), 21. <https://doi.org/10.3390/coatings9010021>
19. T. Sajid, W. Jamshed, F. Shahzad, I. Ullah, R. W. Ibrahim, M. R. Eid, et al., Insightful into dynamics of magneto Reiner-Philippoff nanofluid flow induced by triple-diffusive convection with zero nanoparticle mass flux, *Ain Shams Eng. J.*, **14** (2022), 101946. <https://doi.org/10.1016/j.asej.2022.101946>
20. T. Sajid, W. Jamshed, F. Shahzad, M. A. Aiyashi, M. R. Eid, K. S. Nisar, et al., Impact of Maxwell velocity slip and Smoluchowski temperature slip on CNTs with modified Fourier theory: Reiner-Philippoff model, *Plos One*, **16** (2021), e0258367. <http://doi.org/10.1371/journal.pone.0258367>
21. M. Tahir, A. Ahmad, Impact of pseudoplasticity and dilatancy of fluid on peristaltic flow and heat transfer: Reiner-Philippoff fluid model, *Adv. Mech. Eng.*, **12** (2020). <https://doi.org/10.1177/1687814020981184>
22. S. U. S. Choi, J. A. Eastman, *Enhancing thermal conductivity of fluids with nanoparticles*, San Francisco: ASME International Mechanical Engineering Congress and Exposition, 1995, 12–17.
23. S. U. S. Choi, J. A. Eastman, *Enhancing thermal conductivity of fluid with nanofluids*, 1995.
24. Y. M. Xuan, Q. Li, Heat transfer enhancement of nanofluids, *Int. J. Heat Fluid fl.*, **21** (2000), 58–64. [https://doi.org/10.1016/S0142-727X\(99\)00067-3](https://doi.org/10.1016/S0142-727X(99)00067-3)
25. J. Buongiorno, Convective transport in nanofluids, *ASME J. Heat Mass Transfer.*, **128** (2006), 240–250. <https://doi.org/10.1115/1.2150834>
26. G. Rasool, N. A. Shah, E. R. El-Zahar, A. Wakif, Numerical investigation of EMHD nanofluid flows over a convectively heated riga pattern positioned horizontally in a Darcy-Forchheimer porous medium: application of passive control strategy and generalized transfer laws, *Waves Random Complex Media*, 2022. <https://doi.org/10.1080/17455030.2022.2074571>
27. A. Shahzad, F. Liaqat, Z. Ellahi, M. Sohail, M. Ayub, M. R. Ali, Thin film flow and heat transfer of Cu-nanofluids with slip and convective boundary condition over a stretching sheet, *Sci. Rep.*, **12** (2022), 14254.
28. A. A. Memon, S. Murtaza, M. A. Memon, K. Bhatti, M. Haque, M. R. Ali, Simulation of thermal decomposition of Calcium Oxide in water with different activation energy and the high Reynolds number, *Complexity*, **2022** (2022), 3877475. <https://doi.org/10.1155/2022/3877475>

29. A. F. Abu-Bakr, T. Kanagawa, A. K. Abu-Nab, Analysis of doublet bubble dynamics near a rigid wall in ferrofluid nanofluids, *Case Stud. Therm. Eng.*, **34** (2022), 102060. <https://doi.org/10.1016/j.csite.2022.102060>
30. K. Sajjan, N. A. Shah, N. A. Ahammad, S. S. K. Raju, M. D. Kumar, W. Weera, Nonlinear Boussinesq and Rosseland approximations on 3D flow in an interruption of Ternary nanoparticles with various shapes of densities and conductivity properties, *AIMS Mathematics*, **7** (2022), 18416–18449. <https://doi.org/10.3934/math.20221014>
31. M. Sheikholeslami, D. D. Ganji, Nanofluid flow and heat transfer between parallel plates considering Brownian motion using DTM, *Comput. Methods Appl. Mech. Eng.*, **283** (2015), 651–663. <https://doi.org/10.1016/j.cma.2014.09.038>
32. A. K. Abu-Nab, A. F. Abu-Bakr, Effect of bubble-bubble interaction in Cu-Al₂O₃/H₂O hybrid nanofluids during multibubble growth process, *Case Stud. Therm. Eng.*, **33** (2022), 101973. <https://doi.org/10.1016/j.csite.2022.101973>
33. A. Rauf, N. A. Shah, A. Mushtaq, T. Botmart, Heat transport and magnetohydrodynamic hybrid micropolar ferrofluid flow over a non-linearly stretching sheet, *AIMS Mathematics*, **8** (2023), 164–193. <https://doi.org/10.3934/math.2023008>
34. S. Hina, T. Hayat, S. Asghar, A. A. Hendi, Influence of compliant walls on peristaltic motion with heat/mass transfer and chemical reaction, *Int. J. Heat Mass Transfer*, **55** (2012), 3386–3394. <https://doi.org/10.1016/j.ijheatmasstransfer.2012.02.074>
35. N. Iftikhar, A. Rehman, Peristaltic flow of an Eyring Prandtl fluid in a diverging tube with heat and mass transfer, *Int. J. Heat Mass Transfer*, **111** (2017), 667–676. <https://doi.org/10.1016/j.ijheatmasstransfer.2017.04.013>
36. M. M. Bhatti, A. Zeeshan, R. Ellahi, N. Ijaz, Heat and mass transfer of two-phase flow with electric double layer effects induced due to peristaltic propulsion in the presence of transverse magnetic field, *J. Mol. Liq.*, **230** (2017), 237–246. <https://doi.org/10.1016/j.molliq.2017.01.033>
37. T. Hayat, S. Farooq, B. Ahmad, A. Alsaedi, Homogeneous-heterogeneous reactions and heat source/sink effects in MHD peristaltic flow of micropolar fluid with Newtonian heating in a curved channel, *J. Mol. Liq.*, **223** (2016), 469–488. <https://doi.org/10.1016/j.molliq.2016.08.067>
38. S. Nadeem, T. Hayat, N. S. Akbar, M. Y. Malik, On the influence of heat transfer in peristalsis with variable viscosity, *Int. J. Heat Mass Transfer*, **52** (2009), 4722–4730. <http://doi.org/10.1016/j.ijheatmasstransfer.2009.04.037>
39. T. Hayat, A. Tanveer, A. Alsaedi, Mixed convective peristaltic flow of Carreau-Yasuda fluid with thermal deposition and chemical reaction, *Int. J. Heat Mass Transfer*, **96** (2016), 474–481. <https://doi.org/10.1016/j.ijheatmasstransfer.2016.01.055>
40. M. Tahir, A. Ahmad, S. A. Shehzad, Study of pseudoplastic and dilatant behavior of nanofluid in peristaltic flow: Reiner-Philippoff models, *Chinese J. Phys.*, **77** (2022), 2371–2388. <https://doi.org/10.1016/j.cjph.2022.04.001>
41. G. C. Shit, N. K. Ranjit, Role of slip velocity on peristaltic transport of couple stress fluid through an asymmetric non-uniform channel: Application to digestive system, *J. Mol. Liq.*, **221** (2016), 305–315. <https://doi.org/10.1016/j.molliq.2016.06.002>
42. M. Awais, S. Farooq, T. Hayat, B. Ahmad, Comparative study of silver and copper water magneto nanoparticles with homogeneous-heterogeneous reactions in a tapered channel, *Int. J. Heat Mass Transfer*, **115** (2017), 108–114. <https://doi.org/10.1016/j.ijheatmasstransfer.2017.07.129>

43. K. Vajravelu, S. Sreenadh, R. Saravana, Combined influence of velocity slip, temperature and concentration jump conditions on MHD peristaltic transport of a Carreau fluid in a non-uniform channel, *Appl. Math. Comput.*, **225** (2013), 656–676. <https://doi.org/10.1016/j.amc.2013.10.014>
44. T. Hayat, R. Iqbal, A. Tanveer, A. Alsaedi, Influence of convective conditions in radiative peristaltic flow of pseudoplastic nanofluid in a tapered asymmetric channel, *J. Magn. Magn. Mater.*, **408** (2016), 168–176. <https://doi.org/10.1016/j.jmmm.2016.02.044>
45. T. Hayat, H. Zahir, A. Alsaedi, B. Ahmad, Heat transfer analysis on peristaltic transport of Ree-Eyring fluid in rotating frame, *Chinese J. Phys.*, **55** (2017), 1894–1907. <https://doi.org/10.1016/j.cjph.2017.08.016>



AIMS Press

©2023 the Author(s), licensee AIMS Press. This is an open access article distributed under the terms of the Creative Commons Attribution License (<http://creativecommons.org/licenses/by/4.0>)